Residual gas fluorescence monitor for relativistic heavy ions at RHIC

T. Tsang,[1,*] D. Gassner,[2] and M. Minty[2]

[1]*Instrumentation Division, Brookhaven National Laboratory, Upton, New York 11973, USA*
[2]*Collider Accelerator Division, Brookhaven National Laboratory, Upton, New York 11973, USA*

A residual gas fluorescence beam profile monitor at the Relativistic Heavy Ion Collider (RHIC) has successfully recorded beam images of various species of relativistic heavy ions during FY2012 operations. These fully striped ions include gold, copper, and uranium at 100, 99.9, and 96.4 GeV/n, respectively. Their beam profiles give an independent measurement of the RHIC beam size and emittance. We estimated their corresponding fluorescence cross sections to be 2.1×10^{-16}, 1.8×10^{-17}, and 2.6×10^{-16} cm^2, and obtained their rms transverse beam sizes of 0.36, 0.37, 0.24 mm for gold, copper, and uranium ions, respectively. They are the smallest ion beam width, thus lowest beam emittance, ever produced at RHIC or any other high-energy heavy ion colliders. These extremely small beam sizes may have reached a fundamental limit to residual gas fluorescence based beam profile monitor. Nevertheless, this beam diagnostic technique, utilizing the beam-induced fluorescence from residual gas where hydrogen is still the dominant constituent in nearly all vacuum systems, represents a passive, robust, truly noninvasive, monitor for high-energy ion beams.

PACS numbers: 41.85.Ew, 25.75.−q, 07.60.−j, 33.50.Dq

I. INTRODUCTION

For the first time in FY2012, RHIC successfully collided ^{238}uranium^{92+} on ^{238}uranium^{92+} and ^{64}copper^{29+} on ^{197}gold^{79+} ions in a collider using full 3D stochastic cooling in the longitudinal and both transverse planes [1]. Unlike ^{197}gold, the naturally occurring ^{238}uranium isotope is a highly deformed football-shaped nucleus. This deformation can be used to produce quark-gluon plasma under extreme conditions; and it is important to test this new state of matter at RHIC. On the other hand, colliding ions of two different species of copper and gold gives substantially different luminosities for physics studies. Here, we extended our residual gas fluorescence monitor (RGFM) technique to establish the fluorescence cross sections other than gold ions which we had previously accomplished at 3.85 to 100 GeV/n energy levels [2].

The use of injected gas to enhance the fluorescence signal for beam profile monitors in storage rings, heavy ion accelerators, high-energy proton and low-energy deuteron accelerators has been implemented [3–8], however, it is a somewhat intrusive beam diagnostic method. Alternatively, a residual gas fluorescence beam profile monitor makes use of the passage of relativistic ion beams in a beam chamber to excite only the residual gas molecules that produce fluorescent light when they return to their ground state. This beam diagnostic technique is

passive, robust, truly noninvasive, insensitive to external electromagnetic fields, and is exceptionally simple yet powerful. Although residual gas such as nitrogen has nanosecond short fluorescence decay time and a large cross section [3], normally it is not present in high vacuum systems. To the contrary, the residual amount of hydrogen is always dominant in nearly all high vacuum apparatus, and its ~15 ns fluorescence decay time is sufficiently fast for nearly all beam profile applications [9]. We capture the fluorescence beam image, determine the fluorescence cross section based on its intensity, project the ion beam profile in the vertical plane to determine the beam size and position, calculate the beam emittance, and compare the results to a well established system of ionization profile monitors (IPMs), which also operates on residual gas but is an active electronic device.

II. ION BEAM PROFILE MEASUREMENTS

At the 12 o'clock position of the RHIC, an RGFM optical system is attached to the hydrogen gas jet apparatus. With the hydrogen gas jet turned off, the residual gas pressure of the vacuum chamber reached ~10^{-9} Torr. At this location, two counterpropagating, but noncolliding, beams circulate in the RHIC, named as Blue and Yellow, inadvertently excite the residual gas along their beam paths producing the familiar atomic hydrogen Balmer series lines at the visible wavelengths of 656.3 nm (H_α), 486.2 nm (H_β), 434.1 nm (H_γ), and shorter wavelengths associated with higher energy quantum states. The fluorescence light was captured by achromatic imaging relay optics onto a CCD camera (AVT Allied Vision Technologies, Stingray F145B, 16-bit, 1388 × 1038 pixels, 6.45 μm pixel size) with or

TABLE I.   RHIC run-12 machine parameters.

Mode	U-U	Cu-Au
Energy per nucleon (GeV)	96.4	99.9 Cu/100 Au
$\gamma\beta_{\text{relativistic}}$ function	103.5	107.4
β betatron function at IP12 (meter)	5.0	5.2 Cu/5.0 Au
# of bunch/ring	111	111
# of ions/bunch (maximum)	0.3×10^9	4.0×10^9 Cu/1.3×10^9 Au
# of ions/ring	3.3×10^{10}	4.4×10^{11} Cu/1.4×10^{11} Au
Beam revolution frequency (kHz)	78.189	78.189
Total # of ions per second	2.6×10^{15}	4.5×10^{16} Cu/1.1×10^{16} Au

without spectral filters. We use the measured sensitivity of the camera $\sim 3.87 \times 10^3$ photons/CCD brightness level/mm^2 at 650 nm, together with some RHIC machine parameters (see Table I) to calculate the fluorescence cross sections of all ion beams. Because of limited viewports available, the camera has a 45-degree viewing angle to the beam directions. Thus, the resulting images show a slight skew of the fluorescence beam path, see sketch in Fig. 1. Nonetheless, the projected ion beam profile in the vertical plane of the collider is unambiguously obtained and markedly present only when the ion beams are circulating the RHIC rings.

The achromatic imaging system has an optical field of view of 36.5×27.3 mm^2 with an *in situ* pixel calibration of 26.3 μm/pixel from the known spacing of an internal rf wire cage, and 11.3 mm depth of focus (DOF) on the beam image after taking into account the 45-degree viewing angle. Using ZEMAX to simulate the imaging system, we obtained a 5 μm image resolution; experimentally, by analyzing an image from an *in situ* target we observed object size below 30 μm. Therefore, we note that beam sizes reported here are not limited by the optical resolution of the imaging system and the fluorescence is not saturated.

All beam images are batch processed using IMAGEJ software. First, we perform a background subtraction from an image just before the beam fill, which is an image without beam, to remove nonzero background light generated from various cold cathode vacuum gauges. Subsequently, any beam related fluorescence is captured without any compromise. Second, we execute a despeckle noise reduction to eliminated speckle on some pixels impaired by ionization radiation. Third, we flip and rotate the image to the correct orientation. Finally, we improve the signal-to-noise prior to data analysis by summing 100 Y-projections at the center region of the image. We then plot their beam sizes and perform a Gaussian fit using the IMAGEJ curve fitting routine.

Figures 2(a) and 2(c) show two selected fluorescence beam images of 96.4 GeV/n U-U and 100 GeV/n Cu-Au ion beams at $\sim 60\%$ into their beam time [10]. The designation of ion beam species is unambiguously determined by the starting streak of the fluorescence beam image. The fluorescence intensity is linearly proportional to the residual gas pressure and the bunch intensity of the ion circulating the RHIC rings [9]. Although the intensity of Cu ion is nearly 3 times higher than Au [see Fig. 3(e)], the lower
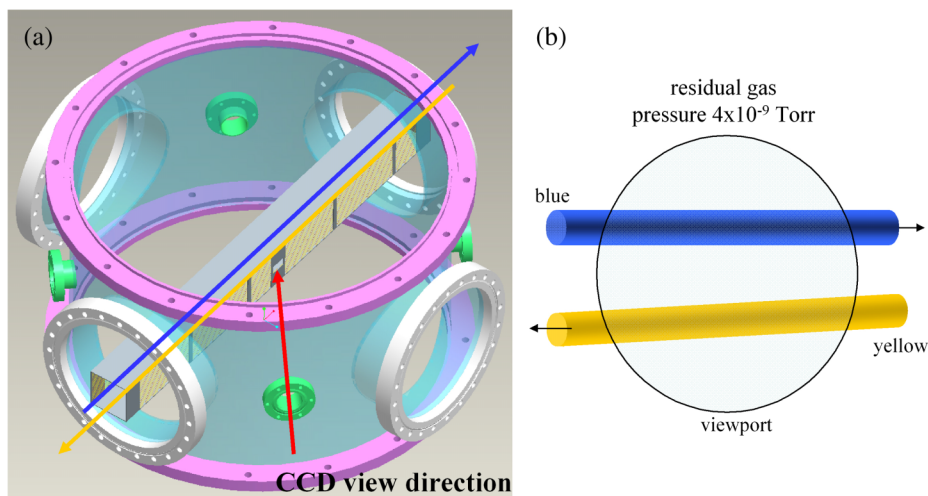
FIG. 1.   (a) Drawing of the interaction chamber and the 45° viewing angle of the CCD. (b) Sketch of the ion beam image orientation showing the slight skew of the beam image as a result of the 45° viewing direction.
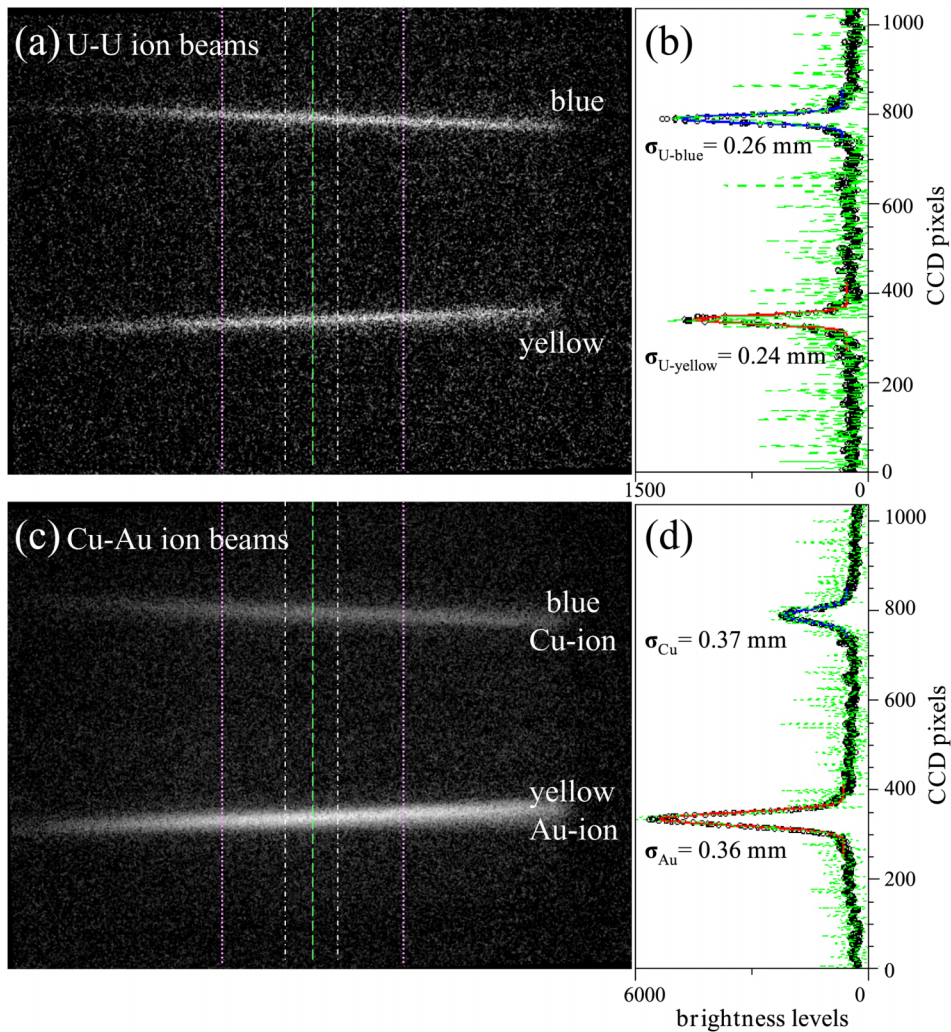
FIG. 2.   (a) Fluorescence profiles of RHIC 96.4 GeV/n U-U ion beams, no spectral filtering, 60 seconds exposure time. The field of view is 36.5 by 27.3 mm (1388 × 1038 CCD pixels), the image area between the dotted magenta lines depicts the depth-of-focus region of the imaging system. (b) Green dashed line: Y-projection at the center of the U-U profile; black open circle: average of 100 Y-projections within the dot-dashed lines region of the image; red and blue solid lines are their respective Gaussian fit for the Yellow and Blue beams. (c) (d) Same as (a) and (b) but for 100 GeV/n Cu-Au ion beams instead. Fitted ion beam width σ values of 9.14, 9.97, 13.8, and 14.1 pixels, with $\chi^2 > 0.96$ confidence level, are obtained for U-Yellow, U-Blue, Au, and Cu beams, respectively; while their beam-beam separations are ~47σ and ~33σ for U-U and Cu-Au ions.

atomic number of Cu actually resulted in a significantly lower yield of fluorescence photons. We note that the fluorescence streaks are sharply focused within the DOF, depicted by the center region between the two magenta lines. Figures 2(b) and 2(d) showed their corresponding beam sizes: the green dashed line is a single Y-projection at the center of the profile, the black open circle is an average of 100 Y-projections within the dot-dashed lines region of the image, and the red and blue solid lines are their respective Gaussian fit. The average of 100 Y-projections improved the signal-to-noise (S/N) ratio by $\sqrt{100}$ compared to that of a single Y-projection. All ion beam profiles have a near Gaussian shape with no pedestals, see Figs. 2(b) and 2(d), therefore, no obvious

beam halo. Previously, by using different narrow band-pass filters to select individual hydrogen Balmer series lines, we determined [9] and reiterate here that hydrogen is the main constituent residual gas in the chamber. We note that residual gases other than hydrogen are also present, but contribute little to this fluorescence process [11]. Even though the fluorescence is collected without spectral filtering, similar beam images are obtained using 656, 486, and 390 nm bandpass filters (H_α, H_β, and H_ζ lines of the Balmer series) with longer exposure. Because of the ~15 ns short fluorescence decay time of hydrogen and its low gas velocity, no image blurring was observed. Ion beam width σ values of 0.24, 0.26, 0.36, and 0.37 mm are obtained for U-Yellow, U-Blue,

T. TSANG, D. GASSNER, AND M. MINTY

Phys. Rev. ST Accel. Beams **16,** 102802 (2013)
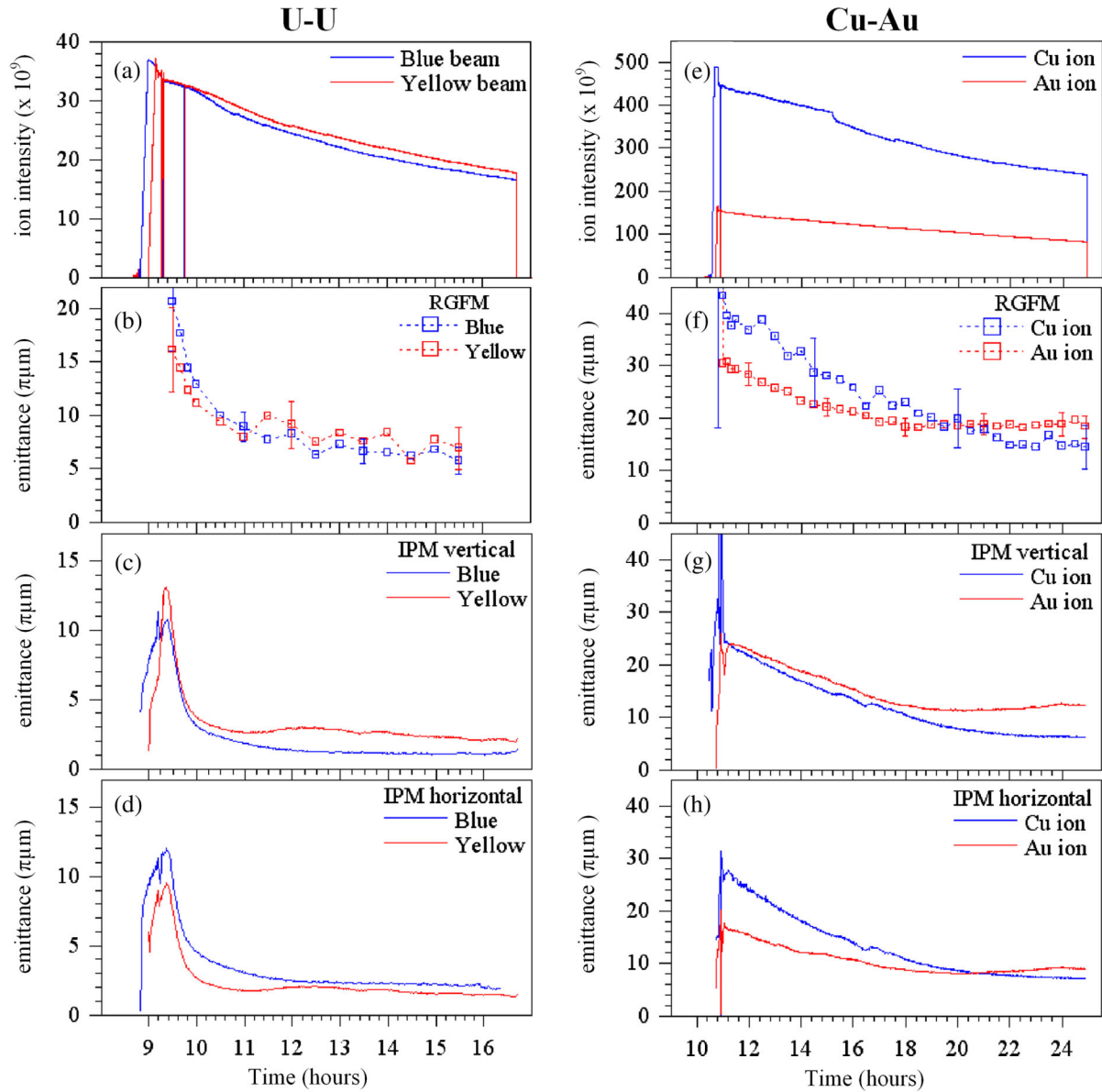
FIG. 3. Representative timeline events of (a) 96.4 GeV/n U-U (e) 100 GeV/n Cu-Au beam ion intensities at injection, ramping, transition, and finally at store. Their corresponding emittance calculated from the beam size measurements of (b) (f) RGFM, (c) (g) IPM vertical, and (d) (h) IPM horizontal. Some representative error bars at a few timeline locations for the RGFM are shown.

Au, and Cu beams, respectively; see Figs. 2(b) and 2(d). They are the smallest ion beam widths, and beam emittances, ever produced at RHIC or any other relativistic heavy ion accelerators. Sufficiently large beam separations of $\sim 47\sigma$ and $\sim 33\sigma$ respectively, for U-U and Cu-Au beams mitigate interbeam coupling; while full implementation of 3D stochastic cooling has alleviated intrabeam scattering and extended beam lifetimes [1]. The reliability and stability of the collider was greatly improved with the fully operational orbit tune and 10 Hz coupling feedback for all acceleration ramps [12].

Even with the improved RHIC operating conditions, the ion beam intensities ultimately decay during the multihour beam storage time due to beam losses from intrabeam collisions, see Figs. 3(a) and 3(e), while beam sizes shrink to a steady state value as a result of stochastic cooling. Therefore, the S/N ratio of the fluorescence beam image drops, leading to a larger uncertainty on the interpretation of beam size. We establish the noise of the beam image as the standard deviation calculated from the brightness levels within a region at the center of the beam image where no fluorescence streaks are presented. It is bounded between the two white dot-dashed lines on the horizontal axis and

from pixels 425–725 on the vertical axis of the images shown in Figs. 2(a) and 2(d). We obtain the peak brightness of each of the ion beams from Figs. 2(b) and 2(d) and then deduce their S/N ratios as 4.2, 5.6, 10.4, and 3.5 for U-Yellow, U-Blue, Au, and Cu beams, respectively. In Sec. IV, we use these S/N ratios to set an upper bound on the error of the beam size and propagate that to the emittance calculation.

III. PHOTON PRODUCTION CROSS SECTIONS

The photon production cross section Ω is an important parameter for the evaluation of the fluorescence monitor. It is experimentally defined as

$$\Omega = \frac{N_{\text{photon}}}{N_{\text{ions}} D_{\text{gas}} L}, \tag{1}$$

where $N_{\text{photon}} / N_{\text{ions}}$ is the photon production efficiency at the source point. D_{gas} is the gas density at the interaction region and equals 3.5×10^7 molecules/cm^3 in a $\sim 10^{-9}$ Torr vacuum. The interaction length L for all ion beams is 24.7 mm (940 CCD pixels) limited by the field of view. By calculating the absolute numbers of fluorescence photons (656 nm photons) collected on the images shown in Fig. 2 and the known number of ions circulating in RHIC over the CCD exposure time, parameters shown in Table I, we deduced their fluorescence cross sections Ω to be 2.1×10^{-16}, 1.8×10^{-17}, and 2.6×10^{-16} cm^2 for 100 GeV/n gold, 99.9 GeV/n copper, and 96.4 GeV/n uranium ions, respectively. If the light production process obeys the Z^2 law from the Bethe-Bloch equation, where $Z_{\text{Au}} = 79$, $Z_{\text{Cu}} = 29$, and $Z_{\text{U}} = 92$, their fluorescence production ratio should be 1.00:0.13:1.35, respectively; experimentally we obtained 1:00:0.09:1.24 instead, but consistent with prediction. Moreover, the cross section of the Au ion is also in qualitative agreement with previous measurements that were done using a different CCD camera [9].

Uranium ions provide the highest fluorescence cross section. A single bunch of 3×10^8 U ions produces only ~ 7 photons at the source point, while a single ring of U ions (total of 3.3×10^{10} ions in 12.7 μs, see Table I) produces ~ 1 photon per revolution reaching the CCD after taking into account the light emission solid angle and the throughput of the imaging system. Therefore, state-of-the-art single-photon sensitive imaging CCD is incapable of measuring the beam profile of a single ion bunch, which might be of interest in analyzing individual bunch to bunch collision data. However, from the beam instrumentation point of view, there is generally no impulsive beam deviation in the time frame of less than a second during routine multihour RHIC storage times. Therefore, beam monitoring with an update rate of seconds is sometimes adequate for certain beam instrumentation systems; and the RGFM can be one such instrument.

IV. EMITTANCE MEASUREMENT AND COMPARISON WITH IPM

Independent beam position monitors at RHIC detected negligible beam movement, if any, within the typical 60-second CCD exposure time. Therefore, the image collected by the RGFM is a valid representation of the ion beam size which can provide beam emittance information to cross-check with other instruments. A system of four ionization profile monitors (IPMs), one for the vertical and another for the horizontal planes of each Blue and Yellow beam, located at the 2 o'clock location are the primary emittance measurement systems in RHIC [13]. Using the measured beam size σ, the known betatron function β, and assuming there is no vertical dispersion or coupling to the horizontal plane, the 95% normalized transverse vertical emittance ε can be calculated using data from the RGFM and IPM as

$$\varepsilon_{\text{RGFM or IPM}} = \frac{6\pi\gamma\beta_{\text{relativistic}}\sigma^2_{\text{RGFM or IPM}}}{\beta_{\text{RGFM or IPM}}}, \tag{2}$$

where $\sigma_{\text{RGFM or IPM}}$ is the rms vertical beam size derived from RGFM or IPM, $\gamma\beta_{\text{relativistic}}$ equals 103.5 and 107.4 for U and Cu or Au beams, β_{RGFM} equals 5 and 5.2 meters while β_{IPM} equals 118.3 and 112.4 meters for Blue and Yellow rings, respectively. We note that beam sizes obtained from the IPM and the RGFM are different because they are located at different RHIC ring positions and have inherently different beam optical properties. The beam emittance can vary on different RHIC beam fills; however, the transverse emittance is a constant value around the RHIC ring for the same beam fills [14] so that comparison can be made among various measurement systems.

Figure 3 displays the timeline events of the complete data shown in Fig. 2 for U-U (left-hand) and Cu-Au (right-hand) ions from injection to store [10]. The bunch intensities, Figs. 3(a) and 3(e), are extracted from respective direct current transformer while the 95% normalized rms beam emittance are derived from RGFM, Figs. 3(b) and 3(f), and IPMs, Figs. 3(c), 3(d), 3(g), and 3(h) and then displayed side by side for comparison. The lower U ion intensity and the smaller fluorescence cross section of Cu ion (lower atomic mass) contribute to a weaker fluorescence light compared to that of Au ion, which subsequently leads to a lower confidence on the interpretation of beam sizes and emittances. Based on the S/N ratio of the beam image, we estimate an upper bound on the error of the RGFM emittances propagated from the beam size calculation. Some representative error bars at a few timeline locations are shown in Figs. 3(b) and 3(f). Larger error bars are prominent on beam start-up due to energy ramping from 24 to ~ 100 GeV and at beam storage end time because of lower beam intensity; both are a consequence of lower fluorescence yield.

It is apparent that both the RGFM and the IPM exhibit steady beam size reduction with time leading to lower emittance and reach a steady state value. But it is also

TABLE II.   Summary of RGFM measurements.

Modes	U-U ions		Cu-Au ions	
RHIC beam	U-Blue	U-Yellow	Cu-Blue	Au-Yellow
Beam width, σ (mm)	0.26	0.24	0.37	0.36
Beam emittance ε (π mm mrad)	5.7–12.5	5.6–11.0	14–27	18–22
Fluorescence cross section (cm^2)	2.6×10^{-16}		1.8×10^{-17}	2.1×10^{-16}

evident that their absolute emittances are in discrepancy. The RGFM consistently measured larger than that of the corresponding IPM (vertical or horizontal) on all ion beam runs. We noted that the total transverse beam emittance equals $1/\sqrt{2}$ on the quadrature sum of vertical and horizontal emittance derived from IPMs is independently cross-checked with the zero degree calorimeters on the PHENIX detector. Nevertheless, both RGFM and IPM report the lowest ion beam emittance ever achieved at RHIC (see Table II) or at any heavy ion colliders.

At the ~20-hour timeline shown in Fig. 3(f), the RGFM Cu-Au emittances cross over. We noted that the relative emittances between the Blue and Yellow beam of the same beam run must be the same for RGFM and IPM. This Cu-Au emittances crossover, Fig. 3(f), was not registered by the vertical IPM, Fig. 3(g), but consistently logged by the horizontal IPM instead, Fig. 3(h). This trend is reproducible for all other ion beam runs, including the U-U ions displayed in Fig. 3(d). We have thoroughly excluded any mishandling of signals, beam skew, or beam coupling. We hypothesize that the vertical and horizontal beam sizes information have intriguingly exchanged upon focusing by quadrupole magnets, which are located upstream and downstream of the RGFM. This finding leads us to uncover some interesting accelerator beam optics behavior. The transverse spatial beam size for a typical RHIC ion beam, recorded at the IPM location, is elliptical rather than spherical. It has an aspect ratio of 1–2 to 1 with the larger dimension in the horizontal rather than the vertical plane. In analogous to conventional light optics, the aspect ratio of a propagating elliptical spatial beam is exchanged at the beam focus, that is, horizontal ↔ vertical. This intriguing beam size exchange phenomena is confirmed from a beam optics code without invoking any beam skew on the quadrupole magnet. Since the RGFM beam emittances are calculated from Eq. (2) using the measured beam sizes, the apparent exchange on the horizontal ↔ vertical beam size at the beam focus leads to a reinterpretation of vertical versus horizontal emittances at the RGFM location. However, the total transverse emittance remains unchanged. More observation and in-depth validation of this hypothesis is needed in future RHIC ion beam runs.

V. PERFORMANCE LIMITS

Using full 3D stochastic cooling, RGFM logged some extremely small beam sizes that require some challenges to interpret. We identified some known beam width broadening effects. First, the skew of the 45-degree viewing angle and the imaging processing (mostly the despeckling process) contribute 1% to 2% overestimation on the beam size. Second, we thoroughly excluded the optical resolution of the imaging system that may contribute to a limit on the beam width. Third, we examined possible beam movement that deviates away from the DOF which would affect the interpretation of the beam width but found it negligible. Four, we scrutinized the influence of the 10 Hz orbit oscillations that may lead to a broadened beam width when CCD exposure times are longer than 100 ms, but found it enlarged only to a few μm. Overall, the cumulative error due to these effects amounts to only a few percent broadening and can not account for the larger ion beam emittance obtained from the RGFM. Finally, experimental confirmation of β_{RGFM} may shed some light on the absolute emittance discrepancy.

We postulated that our RGFM may have reached a fundamental minimum beam size limited by the fluorescence process of the residual gas itself. The mitigation for the discrepancy may require us to introduce a single correction factor that adds in quadrature with the actual beam width to account for the enlarged beam sizes. We scrutinized the influence of the small beam sizes by comparing the emittance obtained from previous years' Au ion beam runs at different beam energies [2], hence, different beam sizes. The result points to a common physical origin: an apparent beam width broadening at higher beam energies (thus smaller beam sizes). Using this methodology, we can qualitatively explain the emittance discrepancy between RGFM and IPM.

VI. CONCLUSION

Beam profile monitors, based on the fluorescence of residual gas excited by the passage of particle beams, are a promising approach for the diagnosis of low-energy to high-energy particle beams. The residual gas fluorescence monitor can provide a real-time guidance for RHIC beam injection, tuning and during the physics experimental program. The nondestructive RGFM is based on beam-induced fluorescence of the residual gas, primarily hydrogen, in the vacuum chamber. The simplicity of this technique substantiates the value of this truly noninvasive, passive, transverse profile measurement of a high-energy particle beam. Even though the ion beam interacts with the

residual gas, it has negligible effects on routine RHIC beam operation. The amount of collected fluorescence light increases linearly with CCD exposure time, beam charge (bunch intensity), and residual gas pressure. Higher atomic weight ion species of the same beam energy produce more fluorescence light photons, see Table II. Most importantly RHIC has achieved a milestone by generating the lowest emittance heavy ion beams; this was confirmed by the RGFM and IPM measurements.

One can gain valuable beam characteristic information immediately by a simple visual inspection of the RGFM beam image. It is highly desirable to have both vertical and horizontal RGFM measurements to pinpoint the position and the size of a beam so that one can uncouple and correct inadvertent beam movements. Once a correction factor for the beam width is identified, the limitation of the RGFM would be on the level of sophistication on photon detection and image processing. Although this can be achieved utilizing a state-of-the-art electron multiplying CCD, so that weak fluorescence images can be collected with photon gain techniques, engineering issues such as radiation shielding, improved image data transfer, and ease of operation must be resolved to realize a near real-time beam monitoring system to better support the operation of particle accelerators.

[1] J. M. Brennan, M. Blaskiewicz, and K. Mernick, in *Proceedings of the International Particle Accelerator Conference (IPAC 2012)* (IEEE, Piscataway, NJ, 2012), paper WEPPP082, p. 2900.

[2] T. Tsang and D. Gassner, in *Proceedings of the Particle Accelerator Conference* (IEEE, New York, 2011), paper MOP210 , p. 492.

[3] A. Variola, R. Jung, and G. Ferioli, Phys. Rev. ST Accel. Beams **10**, 122801 (2007).

[4] A. S. Artemov and S. V. Afanas'ev, Phys. Part. Nucl. **37,** 520 (2006).

[5] F. Becker, C. Andre, P. Forck, D. H. H. Hoffmann, and H. Iwase, in Proceedings of the European Particle Accelerator Conference (EICC, Edinburgh Scotland, 2006), paper TUPCH010, p. 1013.

[6] F. Becker, C. Andre, P. Forck, R. Haseitl, A. Hug, B. Walasek-Höhme, F. Bieniosek, and D. Hoffmann, in *Proceedings of the 9th European Workshop on Beam Diagnostics and Instrumentation for Particle Accelerators, Basel, Switzerland, 2009* (PSI, Basel, 2009), paper TUPB02.

[7] A. Molvik, M. Kireeff Covo, F. Bieniosek, R. Cohen, and A. Faltens, in *Beam Instrumentation and Diagnostics*, edited by P. Strehl (Springer, Berlin Heidelberg, 2006).

[8] J. M. Carmona, I. Podadera, A. Ibarra, A. Bocci, M. C. Jiménez-Ramos, J. García López, and Z. Abou-Haïdar, M. A. G. Álvarez, and B. Fernández, Phys. Rev. ST Accel. Beams **15**, 72801 (2012).

[9] T. Tsang, S. Bellavia, R. Connolly, D. Gassner, Y. Makdisi, T. Russo, P. Thieberger, D. Trbojevic, and A. Zelenski, Rev. Sci. Instrum. **79**, 105103 (2008).

[10] Selected U-U and Cu-Au ion beams are of RHIC beam fill numbers 16857 and 16993, respectively. Many more similar beam fill images converted into time-lapsed videos can be found on the YouTube Website by searching for BNL-CAD.

[11] Preliminary results suggest that remaining beam-induced fluorescence comes from the excitation of the residual oxygen from water vapor producing the familiar atomic oxygen in the NIR of ~777 and ~845 nm).

[12] M. G. Minty, A. J. Curcio, W. C. Dawson, C. Degen, R. L. Hulsart, Y. Luo, G. J. Marr, A. Marusic, K. Mernick, R. J. Michnoff, P. Oddo, V. Ptitsyn, G. Robert-Demolaize, T. Russo, V. Schoefer, C. Schultheiss, S. Tepikian, M. Wilinski, and T. Satogata, in Proceedings of the Particle Accelerator Conference, paper WEOBN1 (Ref. [2]), p. 1394.

[13] R. Connolly, J. Fite, S. Jao, S. Tepikian, and C. Trabocchi, in *Proceedings of the 14th Beam Instrumentation Workshop, Santa Fe, New Mexico* (LANL, Santa Fe, 2010), paper TUPSM010.

[14] A. Zelenski, G. Atoyan, G. Bunce, A. Bazilevshiy, R. Connolly, D. Gassner, R. Gill, H. Huang, G. Mahler, Y. Makdisi, B. Morozov, S. Nemeshure, T. Russo, D. Steski, M. Sivertz, S. Tepikian, R. Todd, and K. Yip, in *Proceedings of the 23rd Particle Accelerator Conference, Vancouver, Canada, 2009* (IEEE, Piscataway, NJ, 2009), paper TH5RFP020.